

# Increased apoptosis of gingival epithelium is associated with impaired autophagic flux in medication-related osteonecrosis of the jaw

Xian Dong, Yang He, Jingang An, Linhai He, Yi Zheng, Xinyu Wang, Jie Wang, Shuo Chen & Yi Zhang

To cite this article: Xian Dong, Yang He, Jingang An, Linhai He, Yi Zheng, Xinyu Wang, Jie Wang, Shuo Chen & Yi Zhang (2023) Increased apoptosis of gingival epithelium is associated with impaired autophagic flux in medication-related osteonecrosis of the jaw, *Autophagy*, 19:11, 2899-2911, DOI: [10.1080/15548627.2023.2234228](https://doi.org/10.1080/15548627.2023.2234228)

To link to this article: <https://doi.org/10.1080/15548627.2023.2234228>

 View supplementary material [↗](#)

 Published online: 21 Jul 2023.

 Submit your article to this journal [↗](#)

 Article views: 212

 View related articles [↗](#)

 View Crossmark data [↗](#)

RESEARCH PAPER



## Increased apoptosis of gingival epithelium is associated with impaired autophagic flux in medication-related osteonecrosis of the jaw

Xian Dong<sup>a</sup>, Yang He<sup>a</sup>, Jingang An<sup>a</sup>, Linhai He<sup>a,b</sup>, Yi Zheng<sup>a</sup>, Xinyu Wang<sup>a</sup>, Jie Wang<sup>a</sup>, Shuo Chen<sup>a</sup>, and Yi Zhang<sup>a</sup>

<sup>a</sup>Department of Oral and Maxillofacial Surgery, Peking University School and Hospital of Stomatology & National Center for Stomatology & National Clinical Research Center for Oral Diseases & National Engineering Research Center of Oral Biomaterials and Digital Medical Devices, Beijing, China;

<sup>b</sup>First Clinical Division, Peking University School Hospital of Stomatology, Beijing, China

### ABSTRACT

Macroautophagy/autophagy has both negative and positive aspects in the development of many diseases. Yet, its exact role and specific mechanism in the onset of medication-related osteonecrosis of the jaw (MRONJ) is still not fully understood. Retarded gingiva healing is the primary clinical manifestation in patients with MRONJ. In this study, we aimed to explore the relationship between autophagy and apoptosis in MRONJ gingival epithelium and search for a method to prevent this disease. First, we examined clinical samples from patients diagnosed with MRONJ and healthy controls, finding that autophagy-related markers MAP1LC3/LC3 and SQSTM1/p62 synchronously increased, thus suggesting that autophagic flux was suppressed in MRONJ. Moreover, mRNA sequencing analysis and TUNEL assay showed that the process of apoptosis was upregulated in patients and animals with MRONJ, indicating autophagy and apoptosis participate in the development of MRONJ. Furthermore, the level of autophagy and apoptosis in zoledronic acid (ZA)-treated human keratinocytes cell lines (HaCaT cells) was concentration dependent *in vitro*. In addition, we also found that RAB7 (RAB7, member RAS oncogene family) activator ML098 could rescue MRONJ gingival lesions in mice by activating the autophagic flux and downregulating apoptosis. To sum up, this study demonstrated that autophagic flux is impaired in the gingival epithelium during MRONJ, and the rescued autophagic flux could prevent the occurrence of MRONJ.

**Abbreviations:** ACTB: actin beta; Baf-A1: bafilomycin A<sub>1</sub>; CASP3: caspase 3; CASP8: caspase 8; CT: computed tomography; DMSO: dimethyl sulfoxide; GFP: green fluorescent protein; HaCaT cells: human keratinocytes cell lines; H&E: hematoxylin and eosin; MAP1LC3/LC3: microtubule-associated protein 1 light chain 3; MRONJ: medication-related osteonecrosis of the jaw; PARP: poly(ADP-ribose) polymerase; RAB7: RAB7, member RAS oncogene family; RFP: red fluorescent protein; SQSTM1/p62: sequestosome 1; TEM: transmission electron microscopy; ZA: zoledronic acid.

### ARTICLE HISTORY

Received 22 August 2022

Revised 21 June 2023

Accepted 3 July 2023

### KEYWORDS

Apoptosis; autophagic flux; gingival epithelium; keratinocytes; medication-related osteonecrosis of the jaw; zoledronic acid

## Introduction

Medication-related osteonecrosis of the jaw (MRONJ) is a rare and painful condition that is difficult to treat. The first case of MRONJ was reported in 2003. The condition is characterized by an area of exposed bone in the mandible and/or maxilla that typically does not heal over 8 weeks [1,2]. Also, the pathophysiological mechanisms associated with MRONJ are very complex and poorly understood [2]. Although soft tissue toxicity has relevant roles in MRONJ pathogenesis [3–5], understanding the molecular mechanisms involved in gingival epithelial injury contributing to the progression of MRONJ is still very limited.

Macroautophagy/autophagy, a necessary biological cellular process responsible for selectively eliminating damaged cellular organelles and protein aggregates, is a lysosome-dependent degradation pathway [6,7]. In healthy human skin, MAP1LC3/LC3 (microtubule associated protein 1 light chain 3), a key autophagosome marker, is expressed in all epidermis layers [8]. Le, et al. demonstrated that keratinocyte

autophagy participates in skin repair by facilitating wound healing and coordinating keratinocyte – fibroblast interaction [9]. However, autophagy also participates the development of various skin diseases, such as viral or bacterial infectious dermatoses, psoriasis, systemic lupus erythematosus, squamous cell carcinoma, and melanoma [10].

Apoptosis is a highly organized and programmed cell death that occurs in multicellular organisms [11,12]. Dysregulation of apoptosis is seen in many diseases [11]. Moreover, apoptosis of osteoclasts, osteoblasts, and gingiva-derived mesenchymal stem cells by bisphosphonates has been recently demonstrated [13–15], implicating that apoptosis may participate in the onset of MRONJ.

Given that gingival epithelium shares similar construct with skin epithelium, we hypothesized that autophagy participate in retarded wound healing in MRONJ. In this study, we explored the relationship between autophagy and apoptosis in MRONJ gingival epithelium and searched for a method to

**CONTACT** Yi Zhang  [zhangyi2000@263.net](mailto:zhangyi2000@263.net); Shuo Chen  [chens@bjmu.edu.cn](mailto:chens@bjmu.edu.cn)  Department of Oral and Maxillofacial Surgery, Peking University School and Hospital of Stomatology & National Center for Stomatology & National Clinical Research Center for Oral Diseases & National Engineering Research Center of Oral Biomaterials and Digital Medical Devices, No.22 Zhongguancun South Avenue, Haidian District, Beijing 100081, P.R. China

 Supplemental data for this article can be accessed online at <https://doi.org/10.1080/15548627.2023.2234228>

prevent this disease. This discovery improves the understanding of the pathogenesis of MRONJ and may provide the potential therapeutic target of this refractory disease.

## Results

### *Gingival autophagic flux is impaired in MRONJ*

All MRONJ patients received debridement. The region of clinical samples was debridement boundary and circled in Fig. S1. Gingival epithelial tissues were collected from patients with MRONJ and healthy persons to assess the levels of autophagy by immunofluorescence staining and western blot. The clinical features of healthy controls and patients diagnosed with MRONJ are presented in Table S1. Both gingival epithelial tissues displayed a relatively normal structure by hematoxylin and eosin (H&E) staining. However, the accumulation of double membrane structures (autophagosomes) was only seen in the MRONJ group (Figure 1A,B).

Then, the autophagy marker LC3 (a direct marker of autophagosome biogenesis) was analyzed [16]. As shown in Figure 1C,D, the LC3 levels were markedly higher in the gingival epithelium of patients with MRONJ than in healthy controls. Moreover, the LC3-II was upregulated in MRONJ gingiva (Figure 1F,G). However, increased LC3 levels do not necessarily mean that the autophagic flux is activated because of the accumulation of autophagosomes; increased LC3 levels may represent autophagy induction or inhibition for deficiency in autophagosome maturation [16]. Thus, SQSTM1/p62 (sequestosome 1), another commonly used autophagy marker whose accumulation reflects intracellular protein aggregation or autophagy dysfunction [17], was detected in the present study. Figure 1C,E show that more SQSTM1 was colocalized with LC3 in MRONJ gingiva vs. control tissue. In addition, the SQSTM1 accumulation in MRONJ was also detected by western blot (Figure 1F,H). Collectively, these data indicate the impairment of autophagic flux in MRONJ gingival epithelium.

### *Impaired autophagic flux by zoledronate is dependent on concentration in vitro*

Human keratinocytes cell lines (HaCaT cells) were treated for 48 h with increasing concentrations of ZA to determine if MRONJ-related key drug bisphosphonates impair autophagic flux. A significant decrease in cell numbers at high concentrations of 25 and 50  $\mu\text{M}$  was found compared with that at a low concentration of 0–1  $\mu\text{M}$  (Figure 2A,B). The cytotoxicity assay also suggested that 10–50  $\mu\text{M}$  ZA were more cytotoxic than 0–5  $\mu\text{M}$  after 48 h (Figure 2C). ZA increased the autophagy-related gene expression in a dose-dependent manner, and these data were consistent with the clinical data shown above. Surprisingly, SQSTM1 was also upregulated along with MAP1LC3B2 (Figure 2D).

For further verification, protein analysis was performed. The results indicated a dose-dependent increase in the LC3-II and SQSTM1, whose effects were consistent with the effect of autophagic flux inhibitor bafilomycin A<sub>1</sub> (Baf-A1) (Figure 2E–G, S2). Furthermore, we found a significant

increase in LC3 (Figure 2H,I). The result of LC3-II accumulation may represent autophagy induction at the early stage or autophagy inhibition at the late stage [16].

For further clarification, HaCaT cells were transfected with RFP (red fluorescent protein)-GFP (green fluorescent protein)-LC3 lentivirus to label autophagosomes with RFP and GFP fluorescence (yellow fluorescence) while labeling autolysosomes with only RFP fluorescence [16]. Upon ZA treatment, yellow fluorescence puncta were significantly increased compared with the control group (Figure 2J,K), which suggested that autophagosome accumulation was due to the inhibition of degradation instead of the induction of generation.

### *Increased apoptosis correlates with the accumulation of LC3 in MRONJ samples*

Considering the critical role of autophagy in the whole life of cells, we evaluated whether the abnormal autophagic flux affects the biological process. mRNA-sequencing studies in gingival epithelium from healthy controls and patients with MRONJ were conducted to clarify the correlation between impaired autophagic flux and MRONJ lesions. In each group, unsupervised hierarchical clustering of the expression data distinguished MRONJ from healthy controls, with minor overlap (Figure 3A). A total of 337 upregulated and 533 downregulated genes were identified based on an analysis of RNA transcriptomes (Figure 3B). Gene ontology (GO) analysis revealed that the upregulated gingival epithelium mRNAs were enriched for biological processes, such as response to variable stimulus, programmed cell death, and apoptotic process (Figure 3C). As autophagy belongs to programmed cell death, the expression of autophagy-related genes was analyzed. Consistently, the key genes mediating autophagosome biogenesis, including ATG4B (autophagy related 4B cysteine peptidase), ATG7 (autophagy related 7), SQSTM1, and MAP1LC3B2, were upregulated compared with those in healthy controls (Figure 3D). Furthermore, enrichment of apoptotic genes was found, including increased expression of BAX (an apoptotic activator) and CASP3 (an apoptotic effector) and decreased expression of BCL2 (an anti-apoptotic gene), as shown in Figure 3E.

Next, immunofluorescence and western blot were conducted on the gingival epithelium to verify whether apoptosis participates in the development of MRONJ. Consistent with the RNA-seq result, the TUNEL assay in MRONJ gingiva revealed more apoptotic cells than in healthy samples (Figure 3F,G). The analysis of apoptosis by western blot showed upregulation of cleaved-CASP3, CASP8 (Figure 3H–J), and pro-apoptotic protein BAX (BCL2 associated X, apoptosis regulator) (Fig. S3). Importantly, the cleaved-CASP3 in MRONJ gingiva was significantly increased and colocalized with LC3 (Figures 3K,L). Thus, we concluded that increased apoptosis correlates with the accumulation of autophagosomes and may have an important role in the onset of MRONJ.

### *Zoledronate induces apoptosis at high concentration*

To further verify whether ZA could induce apoptosis, we detected apoptotic markers at different ZA concentrations *in vitro*. No upregulation of apoptotic protein pro-CASP3

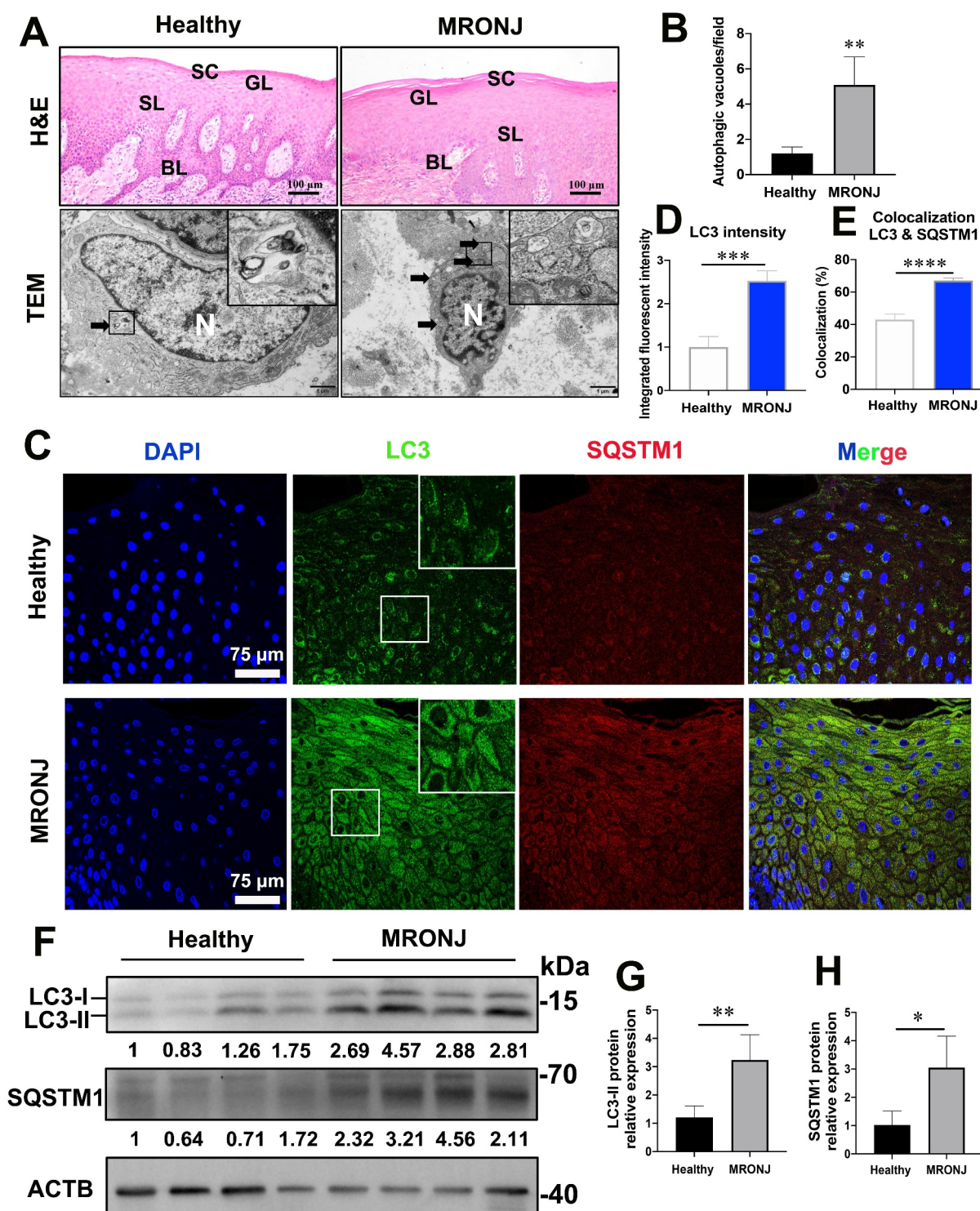


**Figure 1.** Gingival autophagic flux is impaired in MRONJ. (A) Representative images of H&E staining and morphology of autophagic vacuoles of gingival epithelium from a healthy control group and MRONJ group. SC: stratum corneum; GL: granular layer; SL: spinous layer; BL: basal layer. The arrows indicate autophagic vacuoles. N: nucleus. (B) the number of autophagic vacuoles per field ( $n = 4$  individuals for each group). (C) Representative immunofluorescence images of gingival epithelium co-stained with LC3, SQSTM1, and DAPI (yellow indicates LC3 and SQSTM1 colocalized). Scale bar: 75  $\mu\text{m}$ . (D) the mean intensity for LC3 staining ( $n = 4$  individuals for each group). (E) Colocalization of LC3 and SQSTM1. (F-H) Western blot and quantitative analysis of LC3 and SQSTM1 of gingival epithelial tissue in each group ( $n = 4$  individuals for each group). All data are displayed as mean  $\pm$  SEM. \* $p < .05$ ; \*\* $p < .01$ ; \*\*\* $p < .005$ ; \*\*\*\* $p < .0001$ .

was observed, while the expression of pro-apoptotic protein cleaved-CASP3 significantly increased at 25  $\mu\text{M}$  (cells treated at 50  $\mu\text{M}$  ZA resulted in cytotoxic effect). The pro-apoptotic effects of ZA were characterized by significant downregulation of the mitochondrial anti-apoptotic protein (BCL2) ratio

to pro-apoptotic protein (BAX). Furthermore, the expression of cleaved PARP (poly(ADP-ribose) polymerase) was extensively upregulated at 25  $\mu\text{M}$  (Figures 4A,B). Therefore, a ZA concentration of 25  $\mu\text{M}$  was selected for the subsequent cellular experiments.

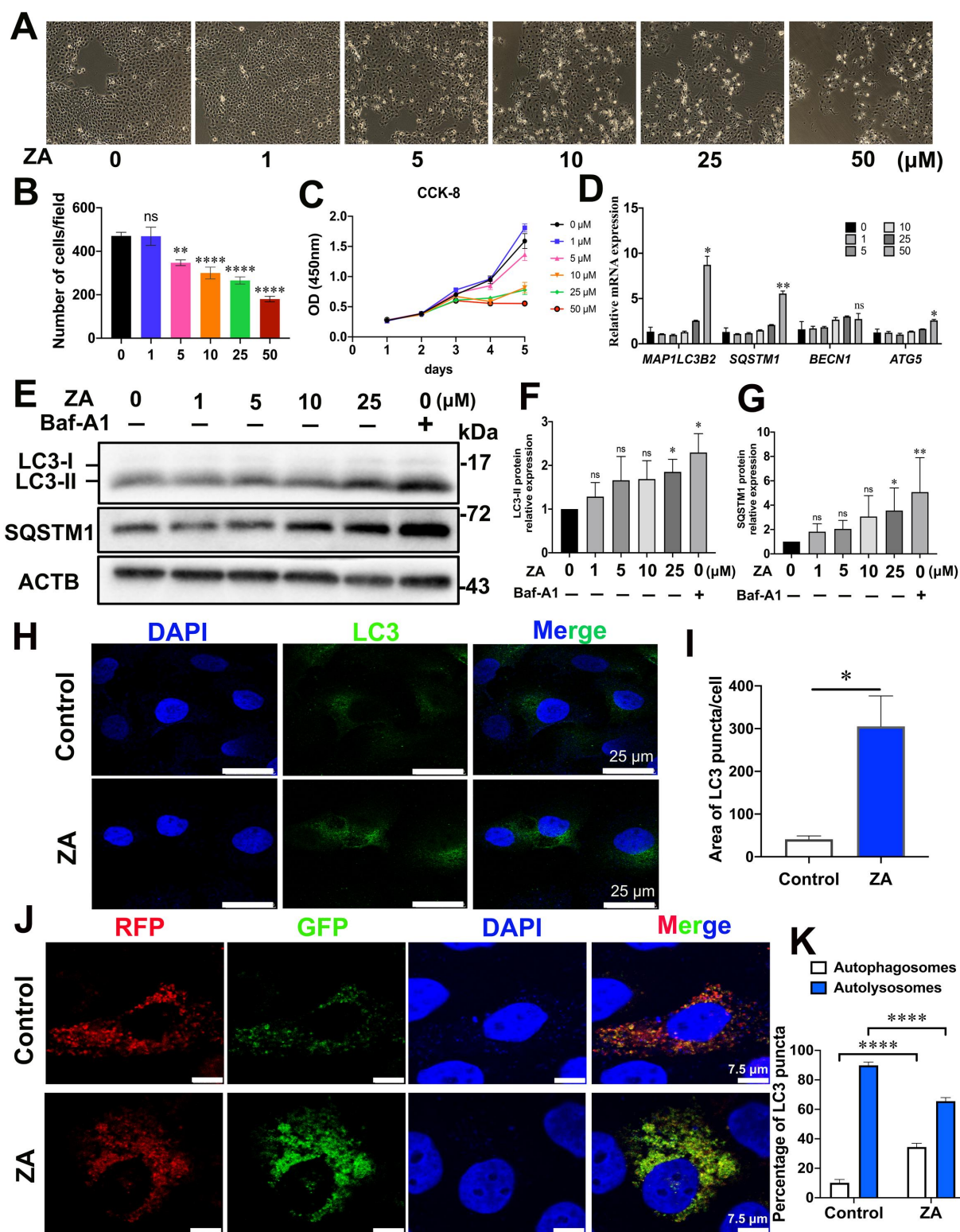


**Figure 2.** Impaired autophagic flux by zoledronate is concentration dependent in vitro. (A and B) HaCaT cells were treated with different concentrations of ZA from 0 to 50  $\mu\text{M}$ . Quantification of cell number per field in different concentrations of ZA is also shown. (C) Effect of ZA on cytotoxicity of HaCaT cells by CCK-8 kit. (D) Autophagy-related genes in HaCaT cells treated with ZA by qPCR. \*  $p < .05$ ; \*\*  $p < .01$  vs. untreated HaCaT cells. (E-G) Western blot and quantitative analysis of the expression of LC3 and SQSTM1 in HaCaT cells after ZA treatment for 48 h. (H) Representative images of LC3 immunostaining in HaCaT cells (control group) and HaCaT cells treated with 25  $\mu\text{M}$  ZA (ZA group). (I) Quantification of the area of LC3 puncta/cells. (J) Representative images of control and ZA-treated HaCaT cells expressing RFP-GFP-LC3. Yellow indicates autophagosomes; RFP (red) indicates autolysosomes in cells. (K) LC3 puncta representing autophagosomes (yellow) and autolysosomes (red) in cells were quantified. All data are displayed as mean  $\pm$  SEM ( $n = 3$ ). \*  $p < .05$ ; \*\*  $p < .01$ ; \*\*\*\*  $p < .0001$ .

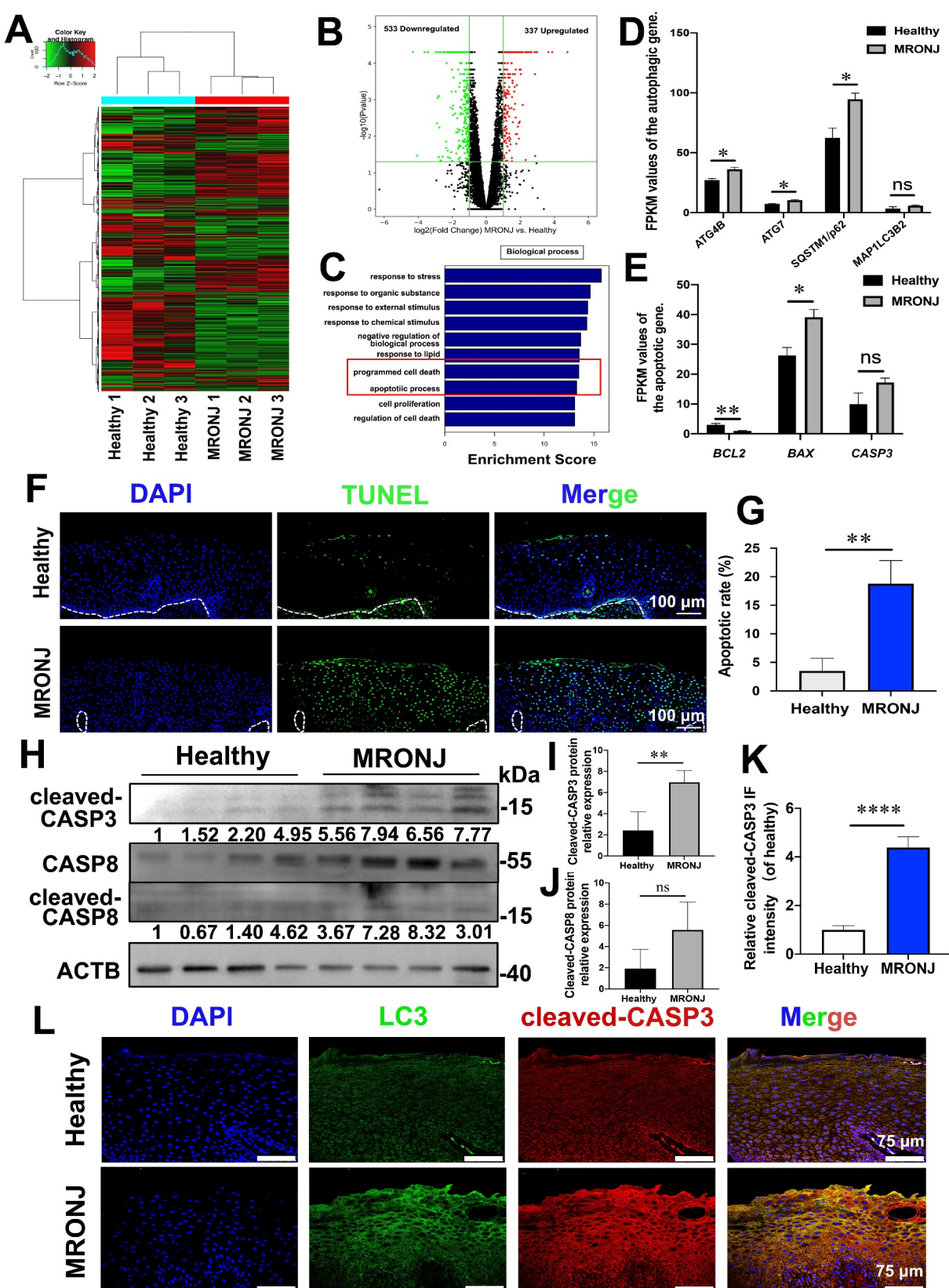


**Figure 3.** mRNA sequencing profiling identified the relative autophagy-related genes and indicated the activation of apoptosis. (A) Clustering analysis of differentially expressed mRNA from the healthy control group (sample 1–3) and MRONJ group (sample 4–6). (B) Volcano plot of differentially expressed mRNA. Green and red represent downregulated and upregulated expression, respectively. (C) GO enrichment analysis identified “upregulation of programmed cell death and apoptotic process” as one of the most marked associated biological processes in the MRONJ group. The FPKM values analysis of the autophagic genes (D) and apoptotic genes (E). (F) Apoptosis of gingival tissue was assayed with TUNEL staining. Scale bar: 100  $\mu\text{m}$ . (G) the quantitative analysis of apoptotic cells. (H–J) Western blot and quantification of protein levels with indicated antibodies of gingival epithelial tissue in each group. (K and L) Representative immunofluorescence images of gingival epithelium co-stained with LC3, cleaved-CASP3, and DAPI. (yellow indicates LC3 and cleaved-CASP3 colocalized). Scale bar: 75  $\mu\text{m}$ . The mean intensity for cleaved-CASP3 staining was analyzed. ( $n = 4$  individuals for each group). \* $p < .05$ ; \*\* $p < .01$ ; \*\*\*\* $p < .0001$ .

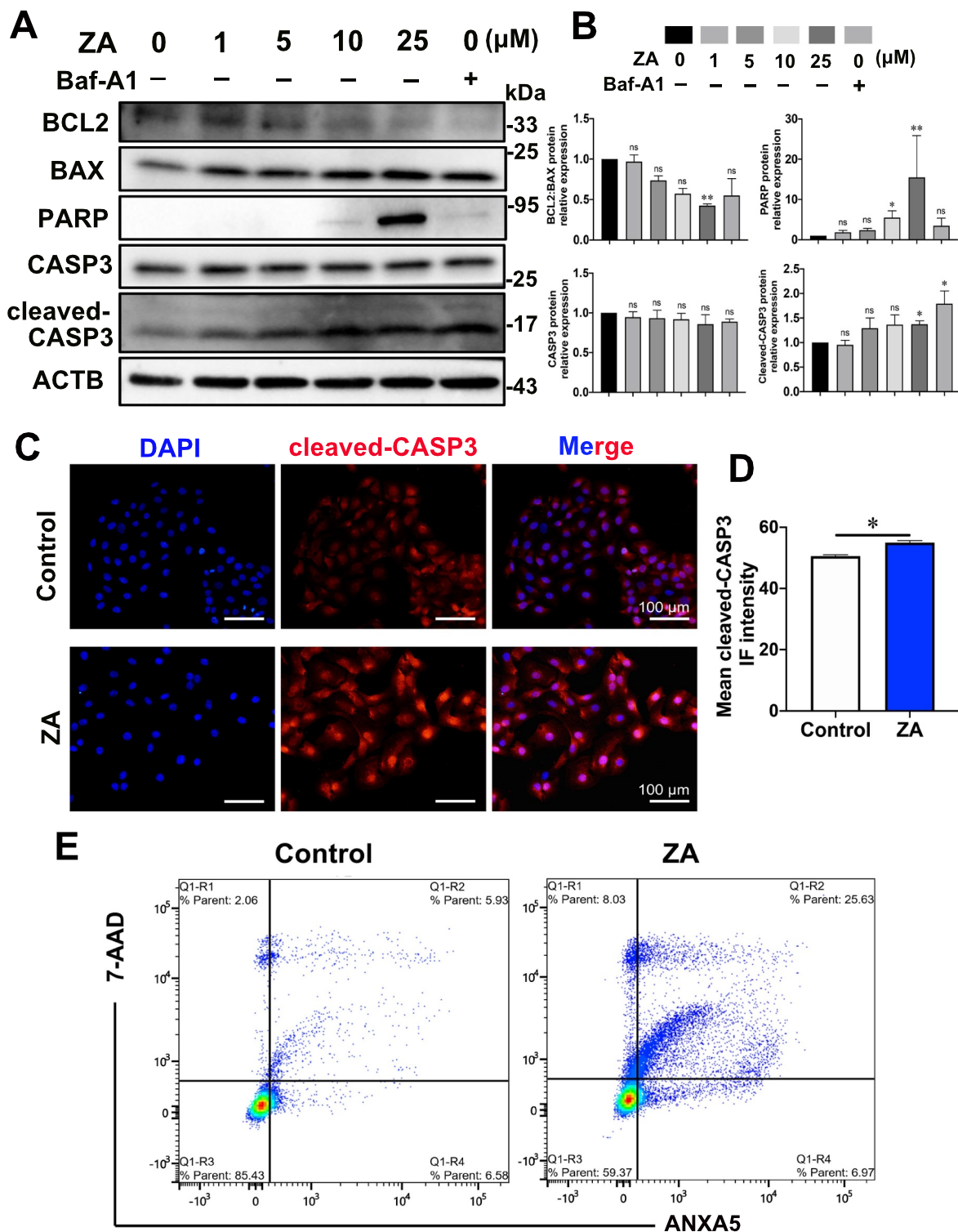


**Figure 4.** Zoledronate induces apoptosis at a high concentration. (A) HaCaT cells were treated with various concentrations of ZA for 48 h. BAX, BCL2, PARP, CASP3, and cleaved-CASP3 were assessed by western blot. (B) Quantitative analysis of the expression of BAX, BCL2, PARP, CASP3, and cleaved-CASP3. (C) Representative images of cleaved-CASP3 and DAPI immunostaining in control and ZA groups. (D) the mean intensity for cleaved-CASP3 staining was analyzed. All data are displayed as mean  $\pm$  SEM ( $n = 3$ ). (E) Apoptosis was determined by flow cytometric analysis in the control and ZA group. \* $p < .05$ ; \*\* $p < .01$ .

Next, cleaved-CASP3 immunofluorescence staining was performed to detect the apoptosis in ZA-treated HaCaT cells. Cleaved-CASP3 was found to be upregulated in the ZA-treated group (Figures 4C,D). Moreover, ANXA5/

annexin V-FITC/7-AAD staining, a more sensitive method for detecting apoptosis, was used to determine the effect of ZA on HaCaT cells. After 48 h of treatment, 32.60% of apoptotic cells (early apoptosis plus late apoptosis) were

detected in ZA-treated cells, while only 12.51% was detected in control cells (Figure 4E). Altogether, ZA can induce HaCaT cell apoptosis at high concentrations, which may correlate to the development of MRONJ.

### The RAB7 activator ML098 alleviates autophagy deficiency and apoptosis in MRONJ

To further explore the specific mechanism of failure in the maturation of autophagosomes, we explored the fusion process between autophagosomes and lysosomes. Previous studies have demonstrated that RAB7, a small GTP binding protein, participates in the lysosome biogenesis, late endosomal-lysosome fusion, and autophagosome maturation [18]. Therefore, the RAB7 activator ML098 was applied to determine its role in ZA-treated epithelial cells. As shown in Figure 5A,B, the level of both LC3-II and SQSTM1 were gradually decreased by ML098 in a dose-dependent manner compared to ZA-treated HaCaT cells. Also, the apoptotic marker cleaved-CASP3 showed similar changes. Yet, no significance of BCL2:BAX was observed, while the level of cleaved PARP was obviously downregulated and was similar to that of the untreated group at the concentration of 5  $\mu$ M (Figure 5A,B). Thus, an ML098 concentration of 5  $\mu$ M was determined for the following cellular experiments.

As shown in Figure 5C,D, immunostaining further demonstrated significant decreases of yellow fluorescence puncta in HaCaT cells transfected with RFP-GFP-LC3 lentivirus when ML098 was added (colocalization rates: ctrl, 65.91% $\pm$ 10.31% vs. ZA, 81.85% $\pm$ 4.64% vs. ML098, 55.86% $\pm$ 8.07%). Moreover, there were more apoptotic cells in the ZA-treated group (48.62% $\pm$ 3.96%) compared with the untreated group (4.20% $\pm$ 2.45%), while ML098 alleviated the number of apoptotic cells (13.78% $\pm$ 1.53%) (Figure 5E,E).

### ML098 rescues the gingival epithelial lesion of MRONJ by activating autophagic flux

To verify whether ML098 could prevent the occurrence of MRONJ, we further applied ML098 in the MRONJ animal model. First, we induced an MRONJ animal model, as previously described [19]. A schematic diagram of inducing the animal model is shown in Fig. S4A. One week after tooth extraction, the MRONJ group showed incomplete mucosal healing and a lack of epithelial coverage at the alveolar socket (Fig. S4B). Micro-CT (computed tomography) analysis further displayed that bone regeneration was significantly impaired in the MRONJ group compared to the control group (Fig. S4B-D). As expected, the immunostaining of LC3 and SQSTM1 further demonstrated that the late stage of autophagy was blocked (Fig. S4E and S4F).

When the administration of ML098 was at the dosage of 1 mg/kg ( $n=6$ /group), the clinical examinations showed fully gingival closure (Figure 6A); yet, at the dosage of 10 mg/kg, delayed gingival closure was observed (Fig. S5). H&E and Masson's staining further verified that the low dose of ML098 could promote gingival healing in MRONJ animals (Figure 6B,C). Additionally, the micro-CT analysis revealed more new bone regeneration at the alveolar sockets after the

administration of ML098 (Figure 6D). More importantly, the expression of both LC3 and SQSTM1 declined in the ML098-treated group; the levels were close to the sham group (Figure 6E,F). In addition, the ML098-treated group showed fewer apoptotic cells than the MRONJ group (Figure 6G,H), which was consistent with our *in vitro* results. In conclusion, these data suggest that a low dose of RAB7 activator ML098 can induce autophagic flux and rescue the gingival epithelial lesion of MRONJ.

## Discussion

In the present study, we found that impaired autophagic flux associated with apoptotic upregulation in the gingival epithelium was a putative pathogenesis process involved in the development of MRONJ. In addition, our data suggested that RAB7 activator ML098 could effectively rescue the development of MRONJ. The RAB family is the largest part of the RAS-like small GTPase superfamily associated with vesicular trafficking function [20]. Activated GTP-RAB7 has the ability to control several autophagic biological process, such as autophagosome formation, transportation and maturation, as well as lysosome biogenesis [21,22]. To sum up, our results indicated that the RAB7 activator ML098 might be a good candidate for preventing the onset of MRONJ.

As known, autophagy has the capacity of resisting starvation, maintaining cellular homeostasis, and recycling damaged cellular organelles and proteins [23–25]. Suppressive or excessive autophagy could induce abnormal conditions by interacting with apoptosis, inflammation, and immunity [26–28]. Autophagy flux was reported to be impaired in the liver during the development of nonalcoholic fatty liver disease, which could have resulted from increased endoplasmic reticulum stress, leading to apoptosis [29]. In the present study, although the autophagic structures were increased, the level of SQSTM1 protein, another commonly used autophagy marker, was upregulated and highly colocalized with LC3 in MRONJ gingival epithelium, indicating the aggregation of the autophagosome. Notably, autophagy is a highly dynamic process comprising three stages, i.e., autophagosome formation, a fusion of autophagosomes with lysosomes, and degradation [30]. Therefore, autophagosome aggregation may be the result of an activation of autophagosome formation or a blockage of late stages in autophagy, similar to fusion blockage or lysosome dysfunction [31]. In the present study, impaired autophagy flux occurred due to the aberrant degradation of autophagosomes.

The relationship between autophagy and apoptosis in disease is a hot topic; yet, this process is still not fully understood. While some studies reported that autophagy was negatively correlated with apoptosis [32–34], there is increasing evidence that these two are actually positively correlated [35–37]. In the present study, apoptosis was obviously elevated in MRONJ gingival epithelium and ZA-treated cells. Two autophagic proteins (SQSTM1 and BECN1/Beclin1) have been linked to autophagy and apoptosis [38,39]. SQSTM1 is a key autophagosome cargo protein responsible for selective autophagy that can interact directly with several apoptotic pathway proteins, including CASP8, TRAF6 (TNF

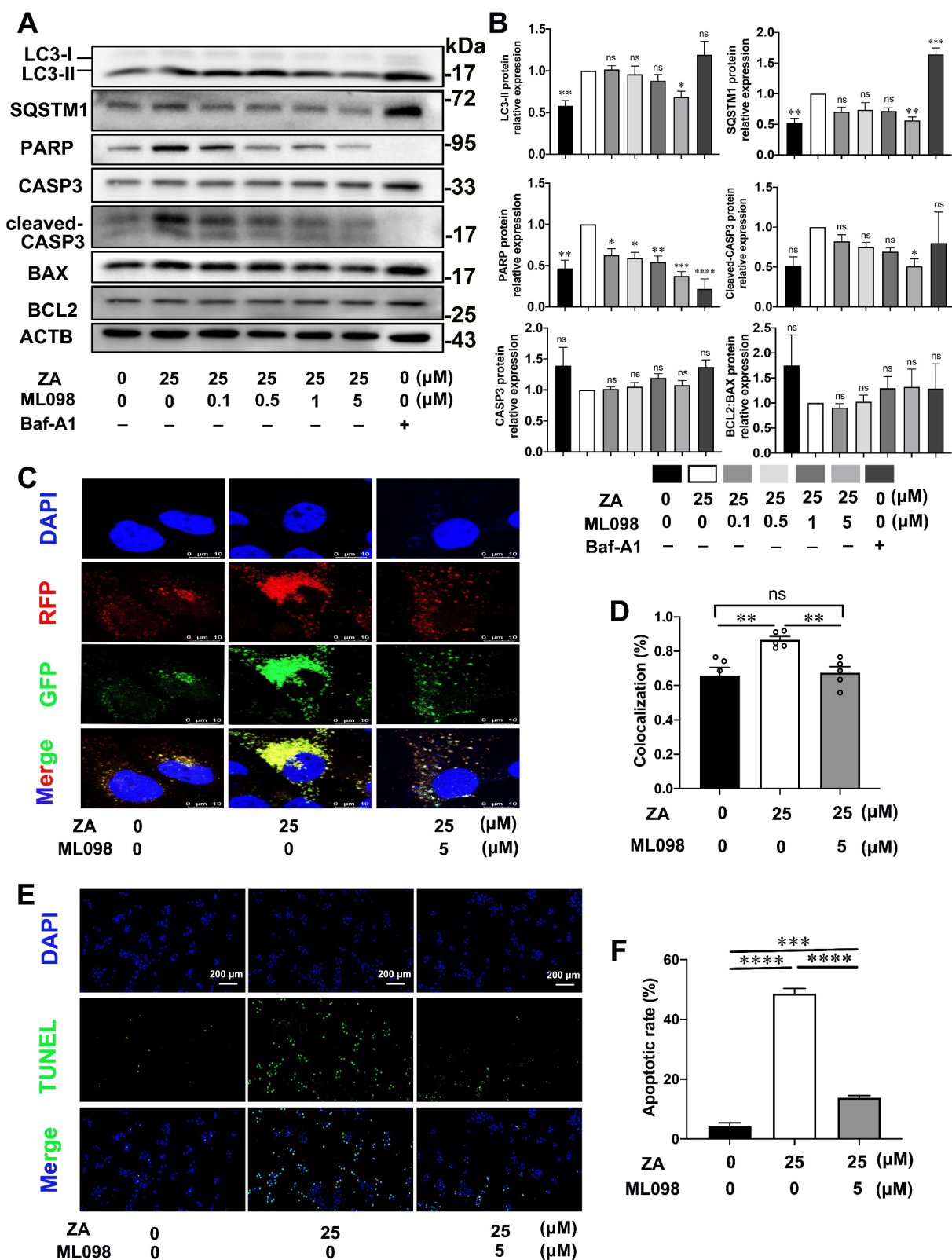


**Figure 5.** The RAB7 activator ML098 alleviates autophagy deficiency and apoptosis *in vitro*. (A and B) Western blot analysis of LC3, SQSTM1, PARP, CASP3, and cleaved-CASP3, BAX, and BCL2 in HaCaT cells after ZA treatment for 48 h and different concentrations of ML098 treatment for 24 h. (C) Representative images of control, ZA-treated, and ML098-treated HaCaT cells expressing RFP-GFP-LC3. Yellow indicates autophagosomes; RFP (red) indicates autolysosomes in cells. (D) the colocalization of RFP and GFP was analyzed. (E and F) Apoptosis was determined by TUNEL staining and analyzed in the control group, ZA group, and ML098 group. All data are displayed as mean  $\pm$  SEM ( $n = 3$ ). \* $p < .05$ ; \*\* $p < .01$ ; \*\*\* $p < .005$ ; \*\*\*\* $p < .0001$ .

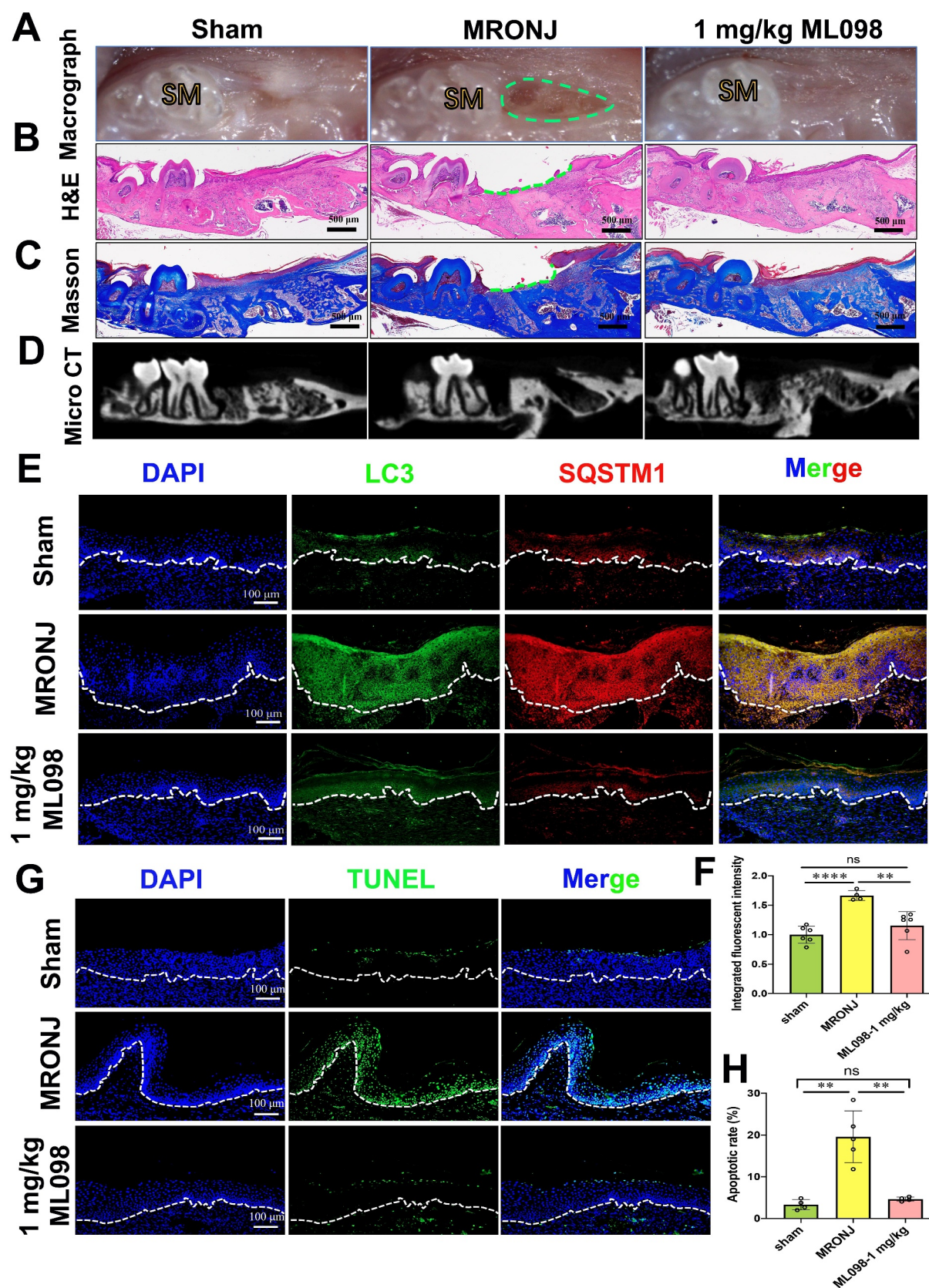


**Figure 6.** The RAB7 activator ML098 can rescue the gingival epithelial lesion of MRONJ by activating autophagic flux. (A-D) Amelioration of MRONJ-like lesion formation by RAB7 activator ML098 intraperitoneal (i.P.) administration ( $n = 6$  per group). SM: Second molar. (E) Representative immunofluorescence images of gingiva co-stained with antibodies against LC3 and SQSTM1. (F) the integrated fluorescent intensity for LC3 staining was analyzed. (G) Apoptosis of gingival tissue was assayed with TUNEL staining. Scale bar: 100  $\mu$ m. (H) the quantitative analysis of apoptotic cells. All data are displayed as mean  $\pm$  SEM. \*\* $p < .01$ ; \*\*\* $p < .005$ .

receptor associated factor 6), and MAPK1/ERK2 (mitogen-activated protein kinase 1) [38]. In the present study, SQSTM1 and CASP8 were elevated in the MRONJ epithelium. However, SQSTM1 is crucial for the activation of CASP8, and conversely, CASP8 can cleave SQSTM1 during apoptosis. Therefore, the exact mechanism between autophagy disorder and apoptosis in MRONJ gingival pathogenesis remains to be determined.

A previous study showed that autophagy integrity is indispensable for epidermal development and differentiation, which may contribute to the pathogenesis of psoriasis if impaired [8]. Furthermore, keratinocyte autophagy can activate keratinocytes and fibroblasts and facilitate wound healing [9]. According to the clinical samples of healthy individuals, autophagy was diffusely expressed in every layer of gingival epithelium rather than the lamina propria. As the keratinocyte HaCaT cell line is a common cell model used to study the pathogenesis of various oral diseases [40–43], we used HaCaT cells for the *in vitro* experiments. However, reduced autophagic flux and increased apoptosis were detected in the gingival epithelium of patients with MRONJ. In addition, sufficient apoptosis was necessary to sustain inflammatory response in wound healing, while excessive apoptosis could have deleterious effects on structure restoration and expose the wound to infection [44]. Thus, the retarded gingival healing of MRONJ may be the result of the loss of the protective function of autophagy and apoptosis for wound healing. Figure 4A,B indicated that zoledronic acid (ZA) not only induced the upregulation of cleaved-CASP3 and cleaved PARP, but also the downregulation of the ratio of mitochondrial anti-apoptotic protein (BCL2) to pro-apoptotic protein (BAX) in a dose-dependent manner. These results suggested that ZA exhibits its apoptotic effect through the CASP3-mediated mechanism in HaCaT cells. Nevertheless, as shown in Figure 5A,B the downregulated expression of BCL2:BAX was not rescued by ML098, which indicated ML098 reduced cellular apoptosis in a CASP3-mediated cleavage of PARP and CASP3 proteins when HaCaT cells treated with ZA.

In conclusion, our study revealed that autophagic flux is impaired, which may associate with apoptosis in the gingival epithelium of MRONJ. External administration of the RAB7 activator can rescue these abnormal processes. Therefore, this study provides insights into the pathogenesis of MRONJ, and RAB7 activator ML098 May be a promising method to prevent the onset of MRONJ.

## Materials and Methods

### Patients

Four patients diagnosed with MRONJ [2] were included in the present study. Detailed clinical information is shown in Table S1. Patients' gingival epithelium, which was the standard debridement boundary [2], was harvested during surgeries at Peking University School and Hospital of Stomatology. In addition, four healthy donors who had underwent cyst curettage or impacted tooth extraction were

included as a control. None of these individuals had tumor metastases nor received radiotherapy. All procedures were approved by the Ethics Committee of the Peking University Health Science Center (PKUSSIRB-202170184).

### MRONJ mouse model

Six-week-old male C57BL/6N mice were purchased from Beijing Vital River Laboratory Animal Technology Co., Ltd and housed under specific pathogen-free conditions. All animal studies were conducted in accordance with the regulations and guidelines of the Ethics Committee of Peking University Health Science Center (LA2022414). Periodontitis was induced with a ligature placed on the first maxillary molar using a 5–0 suture. Next, mice were divided into two groups (six mice per group): the MRONJ group and Control group. MRONJ group was administered with ZA (zoledronate, 1 mg/kg; Sigma-Aldrich, SML0223) once a day in MRONJ group, while the control mice were injected with the same volume of physiological saline. Two weeks after i.p. injection, maxillary first molars were extracted. One week after tooth extraction, maxillae were harvested and fixed in 4% paraformaldehyde.

In the later rescue experiments, RAB7 activator ML098 (1 mg/kg, 3 mg/kg, and 10 mg/kg; Med Chem Express, HY-19800) or DMSO (Sigma-Aldrich, 34869) were i.p. injected for further analysis.

### Transmission electron microscopy (TEM) in gingival samples

The clinical gingiva biopsies were dissected and immediately fixed in 2.5% glutaraldehyde 2 h at 4°C and then rinsed in 0.18 M sucrose (Sigma-Aldrich, 573113) solution for 1 h. The samples were postfixed in 1% osmium tetroxide (Sigma-Aldrich, 1.24505) for 60 min at 4°C, dehydrated in concentrated acetone (50%, 70%, 90%, and 100%) for 15 min, and embedded (Leica; EM UC7, Austria). Ultra-thin sections were examined under the transmission electron microscope (Leica; JEM1400).

### Culture of HaCaT cells and transfection

HaCaT cells were obtained from the central laboratory of Peking University School and Hospital of Stomatology. Cells were cultured in Dulbecco's modified Eagle's medium (DMEM; Gibco, 11995065) supplemented with 10% FBS (Sigma-Aldrich, F8687) and antibiotics – antimycotics (Gibco, 15240062) at 37°C in a humidified atmosphere with 5% CO<sub>2</sub> for 24 h.

Cells were divided into three groups: the ZA group, the Control group and the Baf-A1 group: ZA group received different concentrations of ZA (0, 1, 5, 10, 25, and 50 μM) for 48 h to detect the effect of ZA on HaCaT cells; the Control group was treated with the same volume of physiological saline. the Baf-A1 group was treated with 100 nM bafilomycin A<sub>1</sub> (Selleck, S1413) for 16 h.

The HaCaT cells were infected with RFP-GFP-LC3 retrovirus (GENE[Shanghai], GCD0292404; RFP-GFP-LC3

IRES-Puromycin) at an MOI of 20. Twelve hours after transfection, the transfection medium was replaced with a complete medium. After 72 h, the cells were treated with 2  $\mu\text{g}/\text{mL}$  puromycin (Selleck, S7417) for three days to purify the infected cells. Then, the infected cells were treated with ZA and viewed by fluorescence microscopy. In the later rescue experiments, RAB7 activator ML098 (0, 0.1, 0.5, 1 and 5  $\mu\text{M}$ ) or DMSO were added together with ZA for further analysis.

### Cytotoxicity assay

HaCaT cells were cultured in 96 well plates and treated with ZA from 0–50  $\mu\text{M}$  for 48 h. At each time point, sterile Cell Counting Kit-8 (CCK-8; DOJINDO, CK04) (5 mg/mL) was added to each well and incubated for another 2 h at 37°C. The absorbance at 450 nm was determined using a microplate reader (Thermo Fisher Scientific, USA).

### Immunofluorescence staining

The clinical gingiva biopsies were dissected and fixed in 4% formaldehyde overnight and then dehydrated and embedded in paraffin. Embedded biopsy sections (4  $\mu\text{m}$ ) were deparaffinized and rehydrated, and antigen retrieval was performed by heating for 20 min in a microwave. After blocking with goat serum (ZSGB-BIO, ZLI-9022), samples were incubated with primary antibodies (1:200 dilution) at 4°C overnight and then with secondary antibodies (1:200 dilution) at room temperature for 1 h. Next, the samples were incubated with other primary antibodies at 4°C overnight and secondary antibodies at room temperature for 1 h. Nuclei were then counterstained with DAPI (ZSGB-BIO, ZLI-9557) before imaging. The following primary antibodies were used: LC3 (Abcam, ab48394), SQSTM1/p62 (Cell Signaling Technology, 5114), and cleaved-CASP3 (Cell Signaling Technology, 9664). The following secondary antibodies were used: Alexa Fluor 488 (Abcam, ab150077) and Rhodamine-conjugated antibody (ZSGB-BIO, ZF-0317). After co-immunostaining, images were taken using an LSM710 confocal microscope (Leica, TCS-SP8 STED 3X, Germany).

HaCaT cells were seeded on coverslips and treated with ZA for 24 h. After being washed with PBS (ZSGB-BIO, ZLI-9062), the coverslips were immediately fixed with 4% paraformaldehyde for 20 min and then blocked with goat serum. The primary antibodies were incubated at 4°C overnight and then with secondary antibodies at room temperature for 1 h, followed by DAPI counterstaining.

For TUNEL staining, the sections from human and mouse samples were stained with *In Situ Cell Death Detection Kit* (Roche, 11684795910) following the manufacturer's instruction.

For RFP-GFP-LC3 observation, the transfected cells were seeded on coverslips. After treatment, the cells were immediately fixed with 4% paraformaldehyde for 20 min following counterstaining with DAPI. Images were also acquired using the confocal microscope. For quantitative analysis, the number of LC3 puncta/cells and the ratio of autolysosomes (red fluorescence) versus autophagosomes (yellow fluorescence) were quantified by Image-Pro Plus software (Version 6.0, Media Cybernetics, USA).

### Western blot

Whole-cell extracts and human gingival epithelium specimens were collected using RIPA lysis buffer (Solarbio, R0010) containing proteinase inhibitors (huaxingbio, HX1863) and centrifuged at 14,000 $\times$  g for 20 min at 4°C. Thirty micrograms of protein samples were loaded and separated by 10% SDS-PAGE. After blocking with 1% bovine serum albumin (Sigma-Aldrich, A3294), samples were incubated with primary antibodies (1:1,000 dilution) at 4°C overnight. The following primary antibodies were used: LC3 (Abcam, ab48394), SQSTM1/p62 (Cell Signaling Technology, 5114), BAX (Cell Signaling Technology, 14796), CASP3 (Cell Signaling Technology, 9662), cleaved-CASP3 (Cell Signaling Technology, 9664), cleaved-PARP (Cell Signaling Technology, 5625) and CASP8 (Cell Signaling Technology, 9746). Membranes were then incubated with secondary antibodies (ZSGB-BIO, ZB-2301) and visualized on an electrochemiluminescent detection system.

### Apoptotic analysis

For apoptotic detection, FITC ANXA5/annexin V Apoptosis Detection Kit with 7-AAD (Biolegend, 640922) was used in accordance with the manufacturer's instructions. HaCaT cells were seeded in six-well plates for 12 h and incubated with 25  $\mu\text{M}$  ZA for 48 h. The cells were collected and resuspended cells in ANXA5/annexin V binding buffer at a concentration of  $1 \times 10^7$  cells/mL. Then, 100  $\mu\text{L}$  of cell suspension was transferred in a 5-mL test tube. Next, 5  $\mu\text{L}$  of ANXA5/annexin V-FITC and 5  $\mu\text{L}$  7-AAD were added. Incubation was then conducted at room temperature for 20 min in the dark, and 400  $\mu\text{L}$  of ANXA5/annexin V binding buffer was transferred to each tube. Finally, the results were analyzed by flow cytometry.

### RNA isolation and quantitative real-time polymerase chain reaction (qRT-PCR)

Whole-cell extracts and human gingival epithelium specimens were isolated using TRIzol reagent (Invitrogen, 15596). Total RNA concentrations were measured using the NanoDrop 8000 Spectrophotometer (Thermo Scientific). Complementary DNAs were harvested using the Go Script Reverse Transcription System (Promega, A5003). qRT-PCR was performed with the ABI Prism 7500. The primer sequences used in this study are listed in Table S2.

### mRNA-Seq microarray

RNA high-throughput sequencing was conducted by Cloud-Seq Biotech (Shanghai, China). Briefly, NEBNext rRNA Depletion Kit (New England Biolabs, Inc., E6350) was used to remove the rRNAs in each group ( $n=3$ ) following the manufacturer's instructions. RNA libraries were constructed using NEBNext Ultra™ II Directional RNA Library Prep Kit (New England Biolabs, Inc., E7765) according to the manufacturer's instructions. Libraries were controlled for quality and quantified using the BioAnalyzer 2100 system (Agilent

Technologies, Inc., USA). Consequently, library sequencing was performed on an Illumina NovaSeq 6000 instrument with 150 bp paired-end reads. Paired-end reads were harvested from Illumina NovaSeq 6000 sequencer and quality controlled by Q30. After 3' adaptor trimming and removal of low-quality reads by cutadapt software (v1.9.3), the high-quality clean reads were aligned to the reference genome (UCSC hg19) with hisat2 software (v2.0.4). Then, guided by the Ensembl gtf gene annotation file, cuffdiff software (part of cufflinks) was used to get the gene level FPKM as the expression profiles of mRNA. Fold change and p-value were calculated based on the basis of FPKM, and differentially expressed mRNA was identified. GO and pathway enrichment analysis were performed based on differentially expressed mRNAs.

### Micro-CT scanning evaluation

Two weeks after tooth extraction, maxillae were harvested and fixed in 4% paraformaldehyde for 24 h at room temperature. The maxillae were examined by the micro-CT scanner (Siemens, Inveon MM Gantry-STD 3121, Germany). The parameters were as follows: the X-ray tube voltage was 60 kV, the current was 220  $\mu$ A, the exposure time was 1.5 s. Next, the images were analyzed using matched software (Siemens, COBRA, Germany).

### Statistical analysis

Statistical analysis was performed using unpaired Student's t-test and ANOVA on ABI Prism 7500. P-values less than 0.05 were considered statistically significant.

### Acknowledgements

We wish to thank the Central laboratory of Peking University School and Hospital of Stomatology for providing the research facilities. We thank Pei Fei for the valuable discussion. We also thank Cloud-Seq Biotech Ltd. Co. (Shanghai, China) for the RNA high-throughput sequencing service and the subsequent analysis.

### Disclosure statement

No potential conflict of interest was reported by the authors.

### Funding

The work was supported by the National Natural Science Foundation of China [82101041]; Beijing Natural Science Foundation [7202234]; Beijing Natural Science Foundation [7222223]; the Youth Found of Peking University School and Hospital of Stomatology [PKUSS20200110].

### Data availability statement

The authors confirm that the data supporting the findings of this study are available within the article [and/or] its supplementary materials.

### References

[1] Yarom N, Shapiro CL, Peterson DE, et al. Medication-Related Osteonecrosis of the Jaw: MASCC/ISOO/ASCO Clinical Practice

Guideline. *J Clin Oncol*. 2019 Sep 1;37(25):2270–2290. doi: [10.1200/JCO.19.01186](https://doi.org/10.1200/JCO.19.01186)

[2] Ruggiero SL, Dodson TB, Aghaloo T, et al. American Association of Oral and Maxillofacial Surgeons' Position Paper on Medication-Related Osteonecrosis of the Jaws-2022 Update. *J Oral Maxillofac Surg*. 2022 May;80(5):920–943.

[3] Ziebart T, Halling F, Heymann P, et al. Impact of Soft Tissue Pathophysiology in the Development and Maintenance of Bisphosphonate-Related Osteonecrosis of the Jaw (BRONJ). *Dent J (Basel)*. 2016 Oct 25;4(4):36. doi: [10.3390/dj4040036](https://doi.org/10.3390/dj4040036)

[4] Yuan A, Munz A, Reinert S, et al. Gingival fibroblasts and medication-related osteonecrosis of the jaw: Results by real-time and wound healing in vitro assays. *J Craniomaxillofac Surg*. 2019 Sep;47(9):1464–1474.

[5] Li M, Wang J, Yu Y, et al. Characterization of Mesenchymal Stem Cells Derived from Bisphosphonate-Related Osteonecrosis of the Jaw Patients' Gingiva. *Stem Cell Rev And Rep*. 2022 Jan;18(1):378–394.

[6] Dikic I, Elazar Z. Mechanism and medical implications of mammalian autophagy. *Nat Rev Mol Cell Biol*. 2018 Jun;19(6):349–364. doi: [10.1038/s41580-018-0003-4](https://doi.org/10.1038/s41580-018-0003-4)

[7] Mizushima N, Komatsu M. Autophagy: renovation of cells and tissues. *Cell*. 2011 Nov 11;147(4):728–741. doi: [10.1016/j.cell.2011.10.026](https://doi.org/10.1016/j.cell.2011.10.026)

[8] Akinduro O, Sully K, Patel A, et al. Constitutive Autophagy and Nucleophagy during Epidermal Differentiation. *J Invest Dermatol*. 2016 Jul;136(7):1460–1470.

[9] Qiang L, Yang S, Cui YH, et al. Keratinocyte autophagy enables the activation of keratinocytes and fibroblasts and facilitates wound healing. *Autophagy*. 2020 Sep;18:1–16.

[10] Guo Y, Zhang X, Wu T, et al. Autophagy in Skin Diseases. *Dermatology*. 2019;235(5):380–389. doi: [10.1159/000500470](https://doi.org/10.1159/000500470)

[11] Xu X, Lai Y, Hua ZC. Apoptosis and apoptotic body: disease message and therapeutic target potentials. *Biosci Rep*. 2019 Jan 31;39(1). doi: [10.1042/BSR20180992](https://doi.org/10.1042/BSR20180992)

[12] Grilo AL, Mantalaris A. Apoptosis: A mammalian cell bioprocessing perspective. *Biotechnol Adv*. 2019 May - Jun;37(3):459–475. doi: [10.1016/j.biotechadv.2019.02.012](https://doi.org/10.1016/j.biotechadv.2019.02.012)

[13] Manzano-Moreno FJ, Ramos-Torrecillas J, de Luna-Bertos E, et al. Influence of pH on osteoclasts treated with zoledronate and alendronate. *Clin Oral Investig*. 2019 Feb;23(2):813–820.

[14] Yazici T, Kocer G, Naziroglu M, et al. Zoledronic Acid, Bevacizumab and Dexamethasone-Induced Apoptosis, Mitochondrial Oxidative Stress, and Calcium Signaling are Decreased in Human Osteoblast-Like Cell Line by Selenium Treatment. *Biol Trace Elem Res*. 2018 Aug;184(2):358–368.

[15] Li M, Wang J, Yu Y, et al. Characterization of Mesenchymal Stem Cells Derived from Bisphosphonate-Related Osteonecrosis of the Jaw Patients' Gingiva. *Stem Cell Rev Rep*. 2021 Jan;18(1): 378–394

[16] Klionsky DJ, Abdelmohsen K, Abe A, et al. Guidelines for the use and interpretation of assays for monitoring autophagy (3rd edition). *Autophagy*. 2016;12(1):1–222.

[17] Peng H, Yang F, Hu Q, et al. The ubiquitin-specific protease USP8 directly deubiquitinates SQSTM1/p62 to suppress its autophagic activity. *Autophagy*. 2020 Apr;16(4):698–708.

[18] Jin X, Wang K, Wang L, et al. RAB7 activity is required for the regulation of mitophagy in oocyte meiosis and oocyte quality control during ovarian aging. *Autophagy*. 2022 Mar;18(3):643–660.

[19] Kim T, Kim S, Song M, et al. Removal of Pre-Existing Periodontal Inflammatory Condition before Tooth Extraction Ameliorates Medication-Related Osteonecrosis of the Jaw-Like Lesion in Mice. *Am J Pathol*. 2018 Oct;188(10):2318–2327.

[20] Kuchitsu Y, Fukuda M. Revisiting Rab7 Functions in Mammalian Autophagy: Rab7 Knockout Studies. *Cells*. 2018 Nov 19;7(11):215. doi: [10.3390/cells7110215](https://doi.org/10.3390/cells7110215)

[21] Cai CZ, Yang C, Zhuang XX, et al. NRBF2 is a RAB7 effector required for autophagosome maturation and mediates the association of APP-CTFs with active form of RAB7 for degradation. *Autophagy*. 2021 May;17(5):1112–1130.

- [22] Guerra F, Bucci C. Multiple Roles of the Small GTPase Rab7. *Cells*. 2016 Aug 18;5(3):34. doi: [10.3390/cells5030034](https://doi.org/10.3390/cells5030034)
- [23] Miettinen Teemu P, Björklund M. Mevalonate Pathway Regulates Cell Size Homeostasis and Proteostasis through Autophagy. *Cell Rep*. 2015;13(11):2610–2620. doi: [10.1016/j.celrep.2015.11.045](https://doi.org/10.1016/j.celrep.2015.11.045)
- [24] Levine B, Kroemer G. Biological Functions of Autophagy Genes: A Disease Perspective. *Cell*. 2019 Jan 10;176(1–2):11–42. doi: [10.1016/j.cell.2018.09.048](https://doi.org/10.1016/j.cell.2018.09.048)
- [25] Klionsky DJ, Petroni G, Amaravadi RK, et al. Autophagy in major human diseases. *Embo J*. 2021 Oct 1;40(19):e108863. doi: [10.15252/embj.2021108863](https://doi.org/10.15252/embj.2021108863)
- [26] Yang H, Wen Y, Zhang M, et al. MTORC1 coordinates the autophagy and apoptosis signaling in articular chondrocytes in osteoarthritic temporomandibular joint. *Autophagy*. 2020 Feb;16(2):271–288.
- [27] Matsuzawa-Ishimoto Y, Hwang S, Cadwell K. Autophagy and Inflammation. *Annu Rev Immunol*. 2018 Apr 26;36(1):73–101. doi: [10.1146/annurev-immunol-042617-053253](https://doi.org/10.1146/annurev-immunol-042617-053253)
- [28] Kuo CJ, Hansen M, Troemel E. Autophagy and innate immunity: Insights from invertebrate model organisms. *Autophagy*. 2018;14(2):233–242. doi: [10.1080/15548627.2017.1389824](https://doi.org/10.1080/15548627.2017.1389824)
- [29] Gonzalez-Rodriguez A, Mayoral R, Agra N, et al. Impaired autophagic flux is associated with increased endoplasmic reticulum stress during the development of NAFLD. *Cell Death Dis*. 2014 Apr 17;5:e1179. doi: [10.1038/cddis.2014.162](https://doi.org/10.1038/cddis.2014.162)
- [30] Zhao YG, Codogno P, Zhang H. Machinery, regulation and pathophysiological implications of autophagosome maturation. *Nat Rev Mol Cell Biol*. 2021 Nov;22(11):733–750. doi: [10.1038/s41580-021-00392-4](https://doi.org/10.1038/s41580-021-00392-4)
- [31] Sergin I, Evans TD, Zhang X, et al. Exploiting macrophage autophagy-lysosomal biogenesis as a therapy for atherosclerosis. *Nat Commun*. 2017 Jun 7;8(1):15750. doi: [10.1038/ncomms15750](https://doi.org/10.1038/ncomms15750)
- [32] Wang Y, Tang M. PM2.5 induces autophagy and apoptosis through endoplasmic reticulum stress in human endothelial cells. *Sci Total Environ*. 2020 Mar 25;710:136397.
- [33] Yao L, Chen H, Wu Q, et al. Hydrogen-rich saline alleviates inflammation and apoptosis in myocardial I/R injury via PINK-mediated autophagy. *Int J Mol Med*. 2019 Sep;44(3):1048–1062.
- [34] Chen HX, Liang FC, Gu P, et al. Exosomes derived from mesenchymal stem cells repair a Parkinson's disease model by inducing autophagy. *Cell Death Dis*. 2020 Apr 27;11(4):288. doi: [10.1038/s41419-020-2473-5](https://doi.org/10.1038/s41419-020-2473-5)
- [35] Di YQ, Han XL, Kang XL, et al. Autophagy triggers CTSD (cathepsin D) maturation and localization inside cells to promote apoptosis. *Autophagy*. 2021 May;17(5):1170–1192.
- [36] Luo Z, Xu X, Sho T, et al. ROS-induced autophagy regulates porcine trophectoderm cell apoptosis, proliferation, and differentiation. *Am J Physiol Cell Physiol*. 2019 Feb 1;316(2):C198–C209. doi: [10.1152/ajpcell.00256.2018](https://doi.org/10.1152/ajpcell.00256.2018)
- [37] Yang L, Guan G, Lei L, et al. Palmitic acid induces human osteoblast-like Saos-2 cell apoptosis via endoplasmic reticulum stress and autophagy. *Cell Stress Chaperones*. 2018 Nov;23(6):1283–1294.
- [38] Gump JM, Thorburn A. Autophagy and apoptosis: what is the connection? *Trends Cell Biol*. 2011 Jul;21(7):387–392. doi: [10.1016/j.tcb.2011.03.007](https://doi.org/10.1016/j.tcb.2011.03.007)
- [39] Fairlie WD, Tran S, Lee EF. Crosstalk between apoptosis and autophagy signaling pathways. *Int Rev Cell Mol Biol*. 2020;352:115–158.
- [40] Li Y, Zhang J, Cheng Z, et al. Adenovirus-Mediated LAMA3 Transduction Enhances Hemidesmosome Formation and Periodontal Reattachment during Wound Healing. *Mol Ther Methods Clin Dev*. 2020 Sep 11;18:291–303. doi: [10.1016/j.omtm.2020.06.001](https://doi.org/10.1016/j.omtm.2020.06.001)
- [41] Ferreira LE, Muniz BV, Dos Santos CP, et al. Comparison of liposomal and 2-hydroxypropyl-beta-cyclodextrin-lidocaine on cell viability and inflammatory response in human keratinocytes and gingival fibroblasts. *J Pharm Pharmacol*. 2016 Jun;68(6):791–802.
- [42] Williams DW, Kim RH. Epithelial cells release IL-36alpha in extracellular vesicles following mechanical damage. *Biochem Biophys Res Commun*. 2022 May 21;605:56–62.
- [43] Zhang J, Wang H, Wang Y, et al. Substrate-mediated gene transduction of LAMA3 for promoting biological sealing between titanium surface and gingival epithelium. *Colloids Surf B Biointerfaces*. 2018 Jan 1;161:314–323. doi: [10.1016/j.colsurfb.2017.10.030](https://doi.org/10.1016/j.colsurfb.2017.10.030)
- [44] Shaikh-Kader A, Houreld NN, Rajendran NK, et al. The link between advanced glycation end products and apoptosis in delayed wound healing. *Cell Biochem Funct*. 2019 Aug;37(6):432–442.